Is Transition Metal Oxide a Must? Moisture-Assisted Oxygen Activation in CO Oxidation on Gold/γ-Alumina†

Cheng Shang and Zhi-Pan Liu*

Shanghai Key Laboratory of Molecular Catalysis and Innovative Materials, Department of Chemistry, Key Laboratory for Computational Physical Sciences (Ministry of Education), Fudan University, Shanghai 200433, China

Received: March 18, 2010; Revised Manuscript Received: May 11, 2010

Although a poor catalyst under dry conditions, γ-Al_2O_3-supported gold (Au/γ-Al_2O_3) turns out to be a superior CO oxidation catalyst under moisture conditions. In this work, extensive density functional theory calculations have been carried out to investigate the physical origin of the moisture promotion effect. By supporting Au strips on the two most stable γ-Al_2O_3 surfaces, namely, the (110) and (100) faces, we show that the majority (110) surface is catalytically inert due to the saturation of Al cationic sites by dissociated H_2O. On the other hand, the minority (100) surface in combination with Au is responsible for CO oxidation activity, where O_2 can adsorb at the Au/γ-Al_2O_3(100) interface with a tilted Au−O−O−Al_{5c} configuration. In the presence of coadsorbed H_2O and CO, the adsorption energy of O_2 reaches to 0.7 eV. We find that H_2O enables the direct dissociation of the reaction intermediate *cis*-OCOO produced by the bimolecular coupling between CO and O_2, whereas an extra cis-to-trans rotation of OCOO is required in the absence of H_2O. In the H_2O-assisted pathway, no atomic oxygen is produced, and the overall barrier is only 0.25 eV, which is 0.28 eV lower than that without H_2O. By electronic structure analyses, we suggest that a modest acidity of the γ-Al_2O_3 (100) surface contributes to the O_2 adsorption, although Al_2O_3 lacks the d-states that were shown to be important for O_2 activation.

1. Introduction

Oxide-supported gold catalyst has received considerable attention in the past decade because it exhibits high activity in many important catalytic conversions.[1−12] The activity of gold-based catalyst was shown to be sensitive to both the morphology of gold and the oxide species. A number of key factors were thus summarized, such as the quantum size effect of the gold particle,[3−6] the local coordination of gold,[7,8] the oxide support effect,[9−11,13−15] and the oxidation state of gold.[2,12,16] On the other hand, it was shown recently that the moisture level in the catalytic system is also crucial to activity. In particular, Au/γ-Al_2O_3 is a poor catalyst for CO oxidation at low moisture levels, but with 3000 ppm H_2O, its activity for CO oxidation can increase by 2 orders of magnitude, being similar to that of Au/TiO_2.[17] The promotional effect of moisture was also identified on Au/TiO_2, Au/Fe_2O_3, Au/MgO (only at high temperatures), and Au/SiO_2.[17−19] Since the moisture does not change the catalyst morphology dramatically, it was believed that the catalytic mechanism may be different with and without H_2O.

Various reaction mechanisms have been proposed to understand the moisture effect, focusing on the role of H_2O on O_2 activation. On Au/γ-Al_2O_3, Costello et al.[20] suggested a mechanism that involves a carbonate-like HCO_3 species, which is formed by CO's reacting with the OH and O atom. The HCO_3 can then decompose to release CO_2. Daté et al.,[17] on the basis of their experimental results on Au/TiO_2 and Au/Al_2O_3, suggested that moisture could promote the dissociation of O_2 to produce atomic O at the interface. On the Au/Fe_2O_3 catalyst, Daniells et al.[18] suggested oxygen vacancy formation on the oxide, which is created after the removal of OH. The vacancy will be later healed by the adsorption and dissociation of O_2. By density functional theory (DFT) calculations, Bongiorno et al.[21−23] proposed a reaction path on Au_8/MgO(100) following the Eley−Rideal mechanism, in which an adsorbed O_2−H_2O complex reacts with a gas-phase CO. Gold can extract negative charge from surface defects and give part of that charge further to O_2 to bind and activate it to O−O*.

Among the Au/oxides systems, the Au/γ-Al_2O_3 system is perhaps the most special one,[17,24,25] since its activity appears to be the most sensitive to the moisture level. The phenomenon is difficult to rationalize under the current knowledge framework. First, γ-Al_2O_3 is an irreducible oxide (similar to MgO and SiO_2), which was traditionally regarded as a poor support for Au. Second, γ-Al_2O_3 is not a transition metal oxide (TMO), which lacks the d-states. The empty d-states were shown to play important roles in activating O_2 for CO oxidation on Au/TiO_2 and Au/ZrO_2.[14,26] To date, it remains unclear that how oxygen is activated on Au/γ-Al_2O_3 catalyst, and more intriguingly, how water promotes the reaction. In this work, we thus choose the Au/γ-Al_2O_3 system as the model system to probe the catalytic role of moisture. We have utilized extensive DFT simulation to map out the possible reaction channels for CO oxidation on Au/γ-Al_2O_3. We show that CO oxidation on Au/γ-Al_2O_3 is governed by the H_2O-assisted reaction mechanism. H_2O promotes the CO oxidation by facilitating the decomposition of a reaction intermediate OCOO without the formation of atomic oxygen.

2. Calculation details

All DFT slab calculation was performed using the SIESTA package with numerical atomic orbital basis sets and Troullier−Martins norm-conserving pseudopotentials.[27−29] The generalized gradient approximation method, known as GGA-PBE, was used as the exchange-correlation functional.[30] A double-ζ plus

† Part of the "D. Wayne Goodman Festschrift".

* Corresponding author. E-mail: zpliu@fudan.edu.cn.

10.1021/jp102477g
Published on Web 06/22/2010

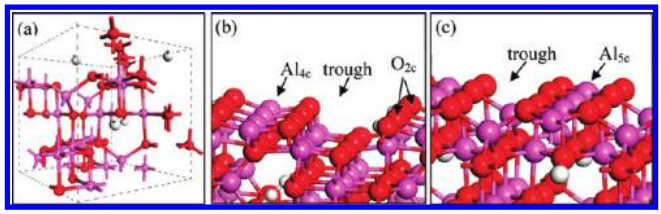

Figure 1. Bulk and surface models of γ-Al_2O_3: (a) defected spinel γ-Al_2O_3 bulk, (b) (110) surface, (c) (100) surface, (O, red; Al, pink; H, white).

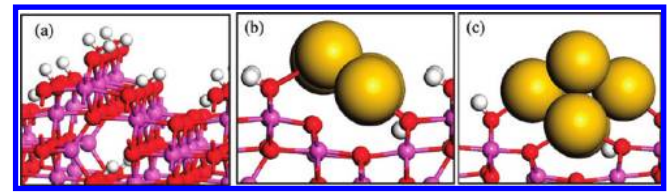

Figure 2. (a) (110) surface covered by dissociated water, (b) one-layer Au strip on the (110) surface, and (c) two-layer Au strip supported on the (110) surface (O, red; Al, pink; H, white; Au, yellow).

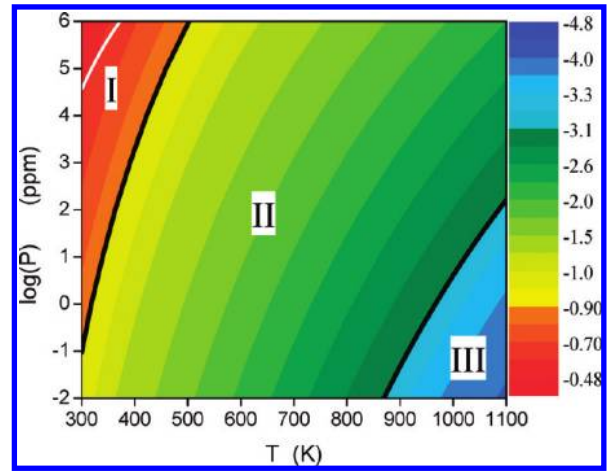

Figure 3. Contour plot of the chemical potential (eV) of the gas phase H_2O at various temperature and pressure conditions. Regions I and II separate at −0.91 eV and the regions II and III separate at −3.10 eV. The white line in region I indicates the chemical potential at the saturated vapor pressure.

polarization basis set was employed.[29,31] An energy shift of 0.01 eV was used to determine the orbital-confining cutoff radii. The energy cutoff for the real space grid used to represent the density was set as 150 Ry. The basis set superposition error was corrected in computing the adsorption energy (E_{ad}) of molecules. $E_{ad}(X)$ is defined as$E_{ad}(X) = E_{substrate} + E_x - E_{x/substrate}$, where E is the DFT total energy; a positive value of E_{ad} means the energy gain during adsorption. The vacuum separation between slabs was more than 16 Å. The geometry relaxation was carried out using the quasi-Newton Broyden method, and the criterion of relaxation for the maximal force on each coordinate was <0.1 eV/Å. For key reaction steps, a criterion of 0.05 eV/Å was utilized to check for convergence, which shows that the difference in adsorption energy or reaction barrier is within 0.05 eV. The transition states of the reactions were searched using our recently developed constrained-Broyden-minimization method[32] and Broyden-Dimer method[33] and confirmed by vibrational frequency calculation via numerical finite difference method. The above calculation setups of SIESTA have been validated by benchmarking some key adsorption energeies with respect to the results from the method based on plane wave basis set. For example, H_2O adsorption energy on clean γ-Al_2O_3(100) is calculated to be 0.91 eV, but it is 0.88 eV from plane wave methods.

Experimentally, γ-Al_2O_3 is an intermediate state transformed from an amorphous or boehmite precursor (boehmite → γ → δ → θ → α[34]). γ-Al_2O_3 appears when boehmite is heated to about 500 °C.[35−37] Because γ-Al_2O_3 is a transition phase, its composition by definition is not fixed, which is known to typically contain 21−31% tetragonal Al and 69−79% octahedral Al.[38,39] In γ-Al_2O_3, hydroxyl is believed to be present due to the incomplete dehydration. Recently, Sohlberg et al.[40] proposed a defected spinel model of γ-Al_2O_3, and the model is also utilized in this work. The optimized cubic cell is shown in Figure 1a ($a = b = c = 8.030$ Å, $\alpha = \beta = \gamma = 90°$). The bulk structure can be visualized as follows. In a spinel magnetite cubic cell, four tetrahedral Fe's [the fractional coordinates 7/8(7/8, 7/8, 7/8), (3/8, 7/8, 7/8), (7/8, 3/8, 7/8), (7/8, 7/8, 3/8)] are replaced by hydrogen atoms that attach to lattice O (i.e., hydroxyl), and the rest Fe are replaced by Al.

The (110) and (100) surfaces have been considered as the possible support for gold since they are the two most stable surfaces of γ-Al_2O_3.[41−43] The bare (110) and (100) surfaces of γ-Al_2O_3 cleaved from the bulk are shown in Figure 1b, c. On the (110) surface, the Al atoms exposed are all four-coordinated (Al_{4c}), and the surface oxygen atoms include both two-coordinated O (O_{2c}) and three-coordinated (O_{3c}) ones; an obvious trough can be seen between two topmost Al−O rows on the surface.[44] On the (100) surface, all the exposed Al atoms are five-coordinated (Al_{5c}), and all the O are O_{3c}. In our slab calculations, the (110) surface is modeled by a p(2 × 1) unit cell (16.06 × 11.36 Å) (Figure 1b). The slab of the (110) surface contains six oxygen layers (Al layers are between oxygen layers) with the bottom four layers fixed at the bulk truncated position. The (100) surface is modeled by a p($\sqrt{2} \times \sqrt{2}$)R45° unit cell (11.36 × 11.36 Å) (Figure 1c). The slab of (100) surface contains four oxygen layers, with the bottom two layers fixed at the bulk truncated position. The convergence of E_{ad} with respect to the layer thickness has been checked by adding two extra oxygen layers, which shows that the calculated E_{ad} of H_2O differs by no more than 0.02 eV. For the (110) surface, only the Γ point was used to sample the first Brillouin zone, and for the (100) surface the **k**-point mesh utilized was (1 × 2 × 1) according to the Monkhorst−Pack scheme.

3. Results

3.1. Au/γ-Al_2O_3(110) System. ***3.1.1. Structure of Au/γ-Al_2O_3(110).*** We first examined the surface phase of the bulk-truncated (110) surface under moisture condition. DFT calculations showed that H_2O can adsorb strongly on the surface (E_{ad} = 1.9 eV), and it can further dissociate into OH and H, which is exothermic by 1.2 eV. In total, 3.1 eV will release to dissociate a H_2O on the surface with respect to a free H_2O at 0 K. After H_2O dissociation, the OH adsorbs at a bridge site between two exposed Al_{4c} and the H sits on a lattice O, as shown in Figure 2a.

To determine the surface phase, we plotted the contour plot of the chemical potential of the gas phase H_2O under different temperature and pressure conditions in Figure 3. The chemical potential is computed with respect to the total energy of free H_2O at 0 K. Figure 3 indicates that the (110) surface is hydrated when the temperature and pressure falls outside the region (III) where the chemical potential of gas phase H_2O is lower than −3.1 eV. Under the typical calcination conditions of a catalyst (e.g., 600 K[17,45]), the (110) surface is thus certainly covered with dissociated H_2O. The strong adherence of H_2O on (110)

can greatly reduce the (110) surface energy, which is in accord with the experiment finding that the (110) surface is the majority surface.[46,47]

Next, we added Au onto the oxide surface. Experimentally, γ-Al_2O_3-supported Au monomer is usually prepared by deposition−precipitation with $HAuCl_4$ under neutral or weak alkaline solution at room temperature. The samples will then be calcined at ~600 K.[17,24,45] This formation procedure can be represented by the following formula:

$$Au(OH)_3 + 3HAl_5O_8 \rightarrow Au(III)/(Al_5O_8)_3 + 3H_2O \quad (1)$$

$$Au(OH)_3 + HAl_5O_8 \rightarrow Au(I)/Al_5O_8 + 2H_2O + 1/2O_2 \quad (2)$$

$$Au(OH)_3 + HAl_5O_8 \rightarrow Au(0)/HAl_5O_8 + 3/2H_2O + 3/4O_2 \quad (3)$$

After we tested the Au monomer, dimer, and trimer species adsorption on various sites of the γ-Al_2O_3(110) surface (the calculation procedure similar to our previous work on ZrO_2[26,48]), we found that the trough of (110) surfaces are the best sites for anchoring Au, and the cationic Au are generally more stable than the neutral Au under typical calcination temperatures. The cationic Au is more stable because the (110) surface is already covered by dissociated H_2O, and thus, by removing the surface H, the cation Au can bond with lattice O. Therefore, two different models have been considered for Au/γ-Al_2O_3(110): namely, one and two-layer Au strips on the oxide. The optimized structures are as shown in Figure 2b and c. Due to the absence of some surface H, these Au strips are overall cationic. In the optimized structures, the Au−Au distance is 2.74−2.87 Å, which is close to the Au bulk lattice constant.

3.1.2. Activity for CO Oxidation. On the Au/γ-Al_2O_3(110) systems, we then explored two possible CO oxidation channels. The first one is the CO reacting with molecular O_2.[13] For CO, it can well adsorb at the edge of Au (E_{ad} = 1.29 eV). However, O_2 adsorbs neither on the Al_2O_3(110) surface nor at the Au/Al_2O_3(110) interface because all Al cations on the (110) surface (after the H_2O dissociation) are capped and saturated. O_2 can only adsorb physically on Au with the optimized O−Au distance being about 2.7 Å. This indicates that the reaction between CO and O_2 cannot follow the Langmuir−Hinshelwood mechanism and is thus ineffcient.[13]

The second possible channel is the CO reacting with the surface OH. Since there is a number of bridging OH groups on γ-Al_2O_3(110) due to the H_2O dissociation, we also investigated the reaction path for the adsorbed CO to react with a surface bridging OH. However, the reaction between CO and the surface OH was found to be impossible because the surface OH is rather inert. Our attempts to optimize the product OCOH at the interface always lead to the breaking of OC−OH bond, and the structure decays back to the initial CO and OH. Overall, there is no feasible reaction channel for CO oxidation in the Au/γ-Al_2O_3(110) model system.

3.2. Au/γ-Al_2O_3(100) System. ***3.2.1. Structure of Au/γ-Al_2O_3(100).*** The (100) is the second stable surface of γ-Al_2O_3, where H_2O was found to adsorb weakly. The E_{ad} of H_2O on bare γ-Al_2O_3(100) was calculated to be 0.91 eV. The H_2O sits on a Al_{5c} with the Al−O bond length being 2.04 Å. The dissociation of H_2O on (100) is a thermoneutral reaction, and the reaction barrier was calculated to be 0.42 eV. After the dissociation, the H bonds with a nearby surface O_{3c}, and the OH sits on the top of Al_{5c}, where the bond distance between Al−OH is 1.78 Å. By comparing to the H_2O chemical potential at the gas phase (Figure 3), we found that H_2O adsorbs on the (100) surface in the region (I), while at typical catalyst calcinations temperatures (e.g., 600 K), the (100) surface can be free of H_2O. Without extra hydroxyls on the (100) surface, the Au on (100) surface is, thus, most likely to be in a charge neutral state.

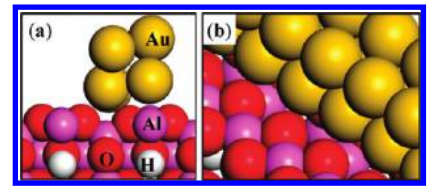

Figure 4. Structure of a 2-layer Au strip on γ-Al_2O_3(100): (a) side view and (b) local view of the interface.

TABLE 1: Adsorption of Oxygen Molecule on Au/γ-Al_2O_3(100)[a]

	O_2	O_2 (+ CO[b])	O_2 (+ H_2O[c])	O_2 (+ H_2O + CO)
E_{ad}/eV	0.50	0.67	0.61	0.70
d_{O-O}/Å	1.35	1.35	1.40	1.41
spin/(μ_B)	0.97	0.96	0.23	0.28
Q (|e|)	−0.77	−0.77	−0.99	−0.94

[a] Q is the Bader net charge[51,52] on the adsorbed O_2. For comparison, the d_{O-O} of free O_2 molecule (triplet) is calculated to be 1.25 Å. [b] E_{ad} of CO is 0.95 eV. [c] E_{ad} of H_2O is 1.00 eV.

On the basis of the facts, we built the supported gold model catalyst as follows. A p($\sqrt{2} \times \sqrt{2}$)R45° unit cell of (100) surface was chosen to anchor the Au strip. We noticed that the lattice of Au and Al_2O_3 can match rather well in the [110] direction (the lattice mismatch is within 1.4% with reference to the bulk lattice constant). A two-layer Au strip was then added onto the (100) surface. By optimizing the Au strip with different initial registration with respect to the substrate, we found that the best adsorption structure for the Au strip is as that shown in Figure 4a, where a row of Au in the first layer is directly above the Al_{5c} (Au−Al distance ~2.85 Å), and the other row of Au in the first layer is at the trough bonding with O_{3c} (Au−O distance ~2.6 Å). The E_{ad} of the Au strip on γ-Al_2O_3(100) is also not high, 0.35 eV per first layer Au atom. This magnitude appears in common for neutral Au on oxide, where 0.46, 0.15, and 0.2−0.3 eV were calculated for Au on rutile TiO_2, anatase TiO_2, and ZrO_2, respectively.[14,49,50] It might be mentioned that the current two-layer Au structure on γ-Al_2O_3(100) mimics those on TiO_2 and ZrO_2,[14,50] which have been utilized to analyze the activity of CO oxidation. The results here on Al_2O_3 can thus be compared systematically with the previous calculations. Experimentally, Goodman and co-workers showed that two-layer Au particles are the most active for CO oxidation on Au/TiO_2.[3−6]

3.2.2. Adsorption of Reaction Species. On the Au/γ-Al_2O_3-(100) model system, we first evaluated the adsorption of the reaction species (CO, O_2 and H_2O) and their interaction in the coadsorption configurations. The results are summarized in Table 1. The adsorption of H_2O at the Au/γ-Al_2O_3 interface (E_{ad} = 1.00 eV) is slightly stronger than on bare γ-Al_2O_3. Molecular oxygen can adsorb at the Au/γ-Al_2O_3(100) interface with its one end resting on Al_{5c} and the other end linking with the Au strip. The E_{ad} of O_2 is 0.50 eV. The interfacial O_2 is still spin-polarized (0.97 μ_B) with a bond length 1.36 Å. Our Bader charge analysis[51,52] shows that the net charge on the adsorbed oxygen is −0.77|e|, which is dominantly transferred

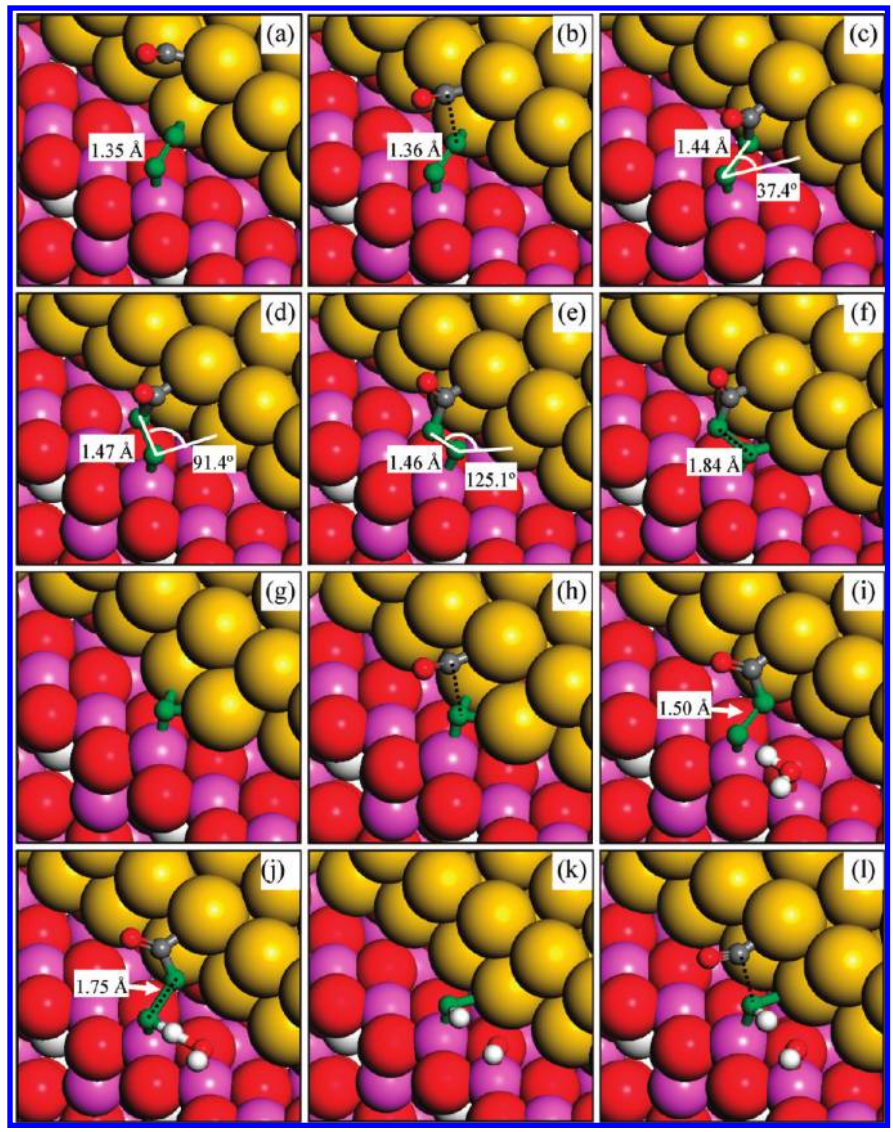

Figure 5. Snapshots of key states in the CO oxidation with and without the presence of H_2O. (a) Coadsorption of CO and O_2, (b) TS of CO reacting with O_2, (c) *cis*-OCOO intermediate, (d) TS for cis-to-trans rotation of OCOO, (e) *trans*-OCOO, (f) TS for O−O bond breaking in *trans*-OCOO, (g) atomic O at the interface, (h) TS for CO reacting with O atom, (i) *cis*-OCOO coadsorption with a H_2O, (j) TS for O−O bond breaking of *cis*-OCOO neighboring with a H_2O, (k) two hydroxyls left at the interface, and (l) TS for CO reacting with OH. The bond lengths of O−O and the angle of O−O−Au (∠OOAu) during cis-to-trans rotation are labeled. (O, red; Al, pink; C, gray; H, white; O of O_2, green).

from the Au strip (overall +0.63|e|). We also considered the other adsorption geometry of oxygen, in which oxygen is parallel to the oxide surface with both oxygen atoms bonding with an Al cation. In this geometry, O_2 adsorbs only weakly (E_{ad}= 0.1 eV). It should be noted that the O_2 adsorption structure on Au/Al_2O_3 interface is different from that on Au/TiO_2 and Au/ZrO_2 systems,[14,50] where the parallel adsorption geometry is preferred generally.

Consistent with previous calculations,[13,14] CO can adsorb on the Au strip, with the E_{ad} being 0.95 eV. The coadsorption of CO with O_2 can improve the E_{ad} of O_2 to 0.67 eV (see Figure 5a). Since there is no change in the bond length, the spin polarization and the net charge of the adsorbed O_2 in the coadsorption system, the increase of the E_{ad} is believed to be due mainly to an electrostatic interaction.

In the presence of H_2O, we found that H_2O can help to increase the E_{ad} of O_2 by ∼0.1 eV, which is apparently caused by the formation of a hydrogen-bonding, HOH−O_2 (1.60 Å). The O_2 bond distance is lengthened to 1.40 Å, and the spin polarization of O_2 is largely quenched in the coadsorbed system. With the nearby H_2O, O_2 becomes more negatively charged by ∼0.22|e|, and the extra electrons are not from H_2O, but still from the Au strip according to Bader charge analysis. It implies that O_2 is further activated due to the H_2O-induced charge transfer. If both H_2O and CO are present, the E_{ad} of O_2 at the interface reaches to 0.70 eV. Considering that the chemical potential of oxygen in the gas phase at 300 K, 1 atm is −0.54 eV with respect to the total energy of free O_2 at 0 K.[53] It indicates that the interfacial O_2 is present under reaction conditions.

3.2.3. CO Oxidation in the Absence of H_2O. We then examined the reaction pathway for CO oxidation in the absence of H_2O. The snapshots of the optimized reaction intermediates are shown in Figure 5a−h, and the determined reaction profile is plotted in Figure 6. The reaction initiates by CO attacking the upper O of molecular O_2 (TS shown in Figure 5b) and forming a *cis*-OCOO complex (Figure 5c, MS_1) at the interface. This bimolecular reaction step is very facile with the computed reaction barrier only 0.14 eV and the step is exothermic by 0.49 eV. At the *cis*-OCOO state, the C of CO bonds with Au, and the lower O of O_2 sits on the top of an Al cation. Due to the formation of the new OC-OO bond, the distance between Au

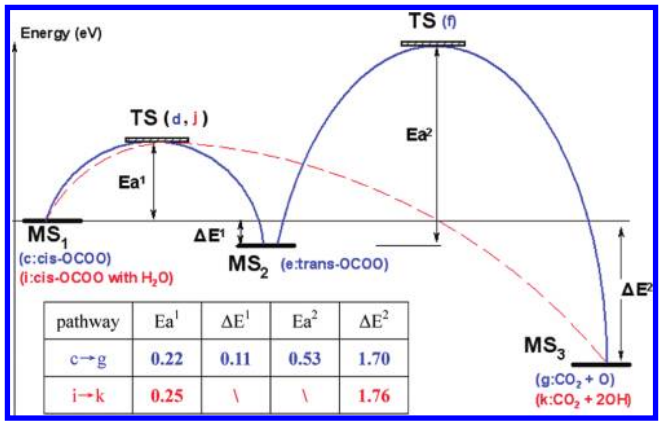

Figure 6. Schematic diagram to illustrate the energetic difference in CO oxidation on Au/γ-Al_2O_3 without (blue solid line) and with H_2O (red dashed line). The structure of states labeled as (c ~ k) can be found in Figure 5. The calculated values (eV) of Ea^1, ΔE^1, Ea^2, ΔE^2 are listed in the inserted table.

and the upper O of O_2 is stretched to 2.8 Å. Next, to produce CO_2, the *cis*-OCOO needs to rotate to a *trans*-OCOO state (TS shown in Figure 5d). The key feature of the trans structure is that the lower O of O_2 bonding with Al also links with Au with the O−Au distance being 2.56 Å (Figure 5e, MS_2). The calculated reaction barrier of the rotation is 0.22 eV. The internal O−O bond at the *trans*-OCOO state can break to release a CO_2, which needs to overcome a reaction barrier of 0.53 eV. After the TS (Figure 5f), a CO_2 molecule is produced with an atomic O left at the interface bonding with both Au and Al (Au−O 2.1 Å). To facilitate the close O−Au contact, the Au atom in the first layer protrudes significantly (outside from the strip, Figure 5g), with its neighboring Au−Au bond distance increasing from 2.93 to 3.28 Å on average, which reflects the weakening of Au−Au metallic bonding. This interfacial O atom can react with another coming CO with a reaction barrier of 0.37 eV (TS shown in Figure 5h).

It should be mentioned that the rotation of the OCOO intermediate is an indispensable step toward CO_2 production. This is because the atomic O is very unstable on the bare Al_2O_3 surface (it is 1.62 eV less stable as compared with $1/2O_2$ in the gas phase) and a direct O−O bond breaking at the *cis*-OCOO state is kinetically prohibited because the leaving O is far away from the Au strip. On the other hand, the atomic O produced from the *trans*-OCOO can be much stabilized due to its simultaneous bonding with Au and Al ($E_{ad}(O) = 0.79$ eV with respect to $1/2O_2$). For the same reason, we also found that the direct dissociation of molecular oxygen is kinetically unlikely at the Au/Al_2O_3 interface.

3.2.4. CO Oxidation in the Presence of H_2O. In the presence of H_2O, the CO oxidation pathway becomes much simpler. The important reaction intermediates in the presence of H_2O is shown in Figure 5i−l, and the identified reaction path is overviewed as follows. Being similar to that without H_2O, the first reaction step—namely, CO + O_2 → *cis*-OCOO (TS shown in Figure 5i)—is facile with a 0.13 eV reaction barrier (the reaction is exothermic by 0.66 eV). In the presence of H_2O, the second step is the direct bond dissociation of the internal O−O bond of the *cis*-OCOO (TS shown in Figure 5j). The reaction barrier of this step is only 0.25 eV. In fact, the key reason that *cis*-OCOO can readily break its O−O bond in the presence of H_2O is the proton passing from H_2O to the lower O of OCOO, which stabilizes the lower O by forming hydroxyl at the interface. When another CO comes, it can react with the hydroxyl directly (TS shown in Figure 5l), and the proton transfer occurs coincidentally to yield CO_2 and H_2O. The reaction barrier of the CO + OH step is only 0.18 eV.

By comparing the reaction pathway with and without H_2O as shown in Figure 6, we can now provide microscopic insight onto the moisture promotion effect. H_2O acts as a cocatalyst in the system. Through the H-bonding at the initial state and the proton-transfer during reaction, H_2O activates the O−O bonds of both adsorbed O_2 and the OCOO intermediate. In the presence of H_2O, the direct cleavage of O−O bond in *cis*-OCOO becomes possible, which saves one elementary step in the reaction profile. Kinetically, this helps to reduce the overall barrier of OCOO decomposition by 0.28 eV (0.53 − 0.25 = 0.28; see Figure 6). ON the basis of Arrhenius law, the presence of moisture can increase the reaction rate by ~10^5 times at 300 K, if assuming the pre-exponential factors are the same.

4. Discussion

4.1. Comparison with Experimental Results. Our results show that CO oxidation on Au/γ-Al_2O_3 follows different reaction pathways with and without H_2O. The presence of H_2O can reduce the overall barrier of CO oxidation by 0.28 eV and thus increase the reaction rate by 5 orders of magnitude at 300 K. However, Daté has suggested that the mechanism of CO oxidation on Au/Al_2O_3 is the same under dry and moisture conditions. Their suggestion is based on the experimental finding that the slope of Arrhenius plots is rather constant when the concentration of moisture increases from 2 to 200 ppm, and the measured apparent activation energies are always ~0.23 eV (22 kJ/mol). It is therefore important to ask whether 2 ppm is a low enough moisture concentration to disallow H_2O adsorption on Au/γ-Al_2O_3.

From Figure 3, we found that the chemical potential of the gas phase H_2O is lower than −1.00 eV only when the moisture concentration is lower than 0.01 ppm at 300 K. Since the H_2O adsorption energy is 1.00 eV at the Au/γ-Al_2O_3(100) interface, one can expect that H_2O is still present on the catalyst at the 2 ppm moisture level under the experimental conditions. Because the reaction rates differ significantly with and without H_2O, CO oxidation on Au/γ-Al_2O_3 will always follow the H_2O-assisted reaction pathway with the moisture level from 2 to 200 ppm. This can rationalize why the similar Arrhenius slopes were observed in experiment. The reaction barrier in the presence of H_2O calculated here (24 kJ/mol) is also consistent with the apparent activation energies in experiment (22 kJ/mol).

It might also be mentioned that carbonate ($-CO_3$, $-HCO_3$) species are not identified in our reaction channels, although the carbonate-involved mechanism has also been suggested in experiment for CO oxidation on Au/γ-Al_2O_3.[20] The presence of carbonate has been observed on Au/TiO_2 catalyst, but no clear evidence of carbonate has been reported on Au/γ-Al_2O_3 systems. Considering that the formation of carbonate is proposed to involve both atomic O and OH at the interface (CO + O + OH → HCO_3),[54] such reaction channels may, indeed, be available for CO oxidation on Au/TiO_2, where the atomic oxygen is present. For Au/γ-Al_2O_3, due to the dominance of the H_2O-assisted reaction channel, only OH species are present in the reaction system, and thus, the possibility to have carbonate species is low.

4.2. Origin of the Activity on γ-Al_2O_3. We are now at a position to address why Au/γ-Al_2O_3 can exhibit as good catalytic activity as Au/TiO_2 but Au supported on other typical irreducible oxides such as MgO and SiO_2 has low activity. Since O_2 adsorption is a known problem on oxides such as Au/MgO,[15] the key issue here is to answer how O_2 is activated on Au/γ-

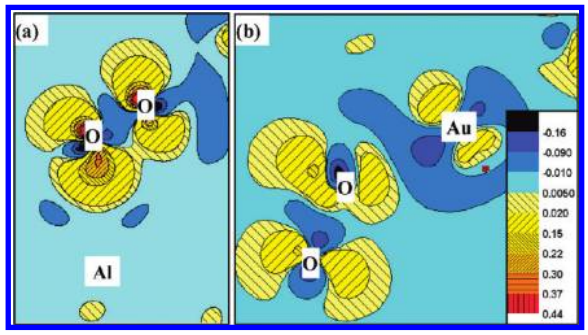

Figure 7. Charge-density-difference contour plots showing the bonding of O_2 at the Au/γ-Al_2O_3(100) interface. Parts a and b are the plots cutting through O_2−Al and O_2−Au bonding planes, respectively. The charge density difference is constructed by subtracting the total electron densities of the O_2 adsorbed model O_2/Au/γ-Al_2O_3(100) from an O_2 and a Au/γ-Al_2O_3 slab, each in the same structure. The unit of charge density is e/Å^3.

Al_2O_3. In fact, we have shown from DFT that O_2 adsorption geometry on Au/γ-Al_2O_3 is different from that on Au/TiO_2 and Au/ZrO_2. At the Au/γ-Al_2O_3 interface, O_2 prefers the one-end Au−O−O−Al_{5c} adsorption geometry (Figure 5a). By contrast, at the Au/TMO, O_2 prefers the parallel adsorption geometry, with both O atoms of O_2 bonding with a TM cation.

To understand further how O_2 interacts with Al_2O_3 and Au, we have analyzed the electronic structure the system before and after the O_2 adsorption. Figure 7 shows the contour plots of the electronic charge density difference, constructed by subtracting the total electron densities of the O_2 adsorbed model (O_2/Au/γ-Al_2O_3) from the separated O_2 and Au/γ-Al_2O_3 slab. The contour planes are through the bonding plans of O_2 with Al and Au, respectively. Figure 7a shows that only polarization of oxygen atom can be seen at the O_2/Al bonding plane, and no covalent bonding (orbital mixing) is found between O and Al. This indicates that the interaction between oxygen and the cationic site of the oxide support is purely electrostatic interaction. On the other hand, the $2\pi^*$ of O_2 can covalently bond with the d orbital of gold, as shown in Figure 7b, where the d orbital of gold toward O_2 depletes while the $2\pi^*$ of O_2 accumulates electron. The bonding picture of O_2 with oxide (Figure 7a) is distinct from that of O_2 adsorption on Au/TMO.[14] For O_2 adsorption on Au/TMO, obvious $2\pi^*(O_2)$−d(TM) bonding can be seen between O_2 and the oxide.

On the basis of electronic structure analyses, we can conclude that O_2 adheres to the Al cation via the acid−base electrostatic interaction, and thus, the one-end adsorption geometry is preferred. For comparison, the E_{ad} of O_2 on Au/Al_2O_3 interface is not high, being around 0.6 eV. On TMO, by contrast, the $2\pi^*$ of O_2 forms the covalent bonding with TM cation the d orbital with a three-center $2\pi^*$-d bonding. The O_2 prefers to adsorb on TM cation with a parallel geometry. With the covalent bonding, the O_2 adsorption on Au/TMO interface is thus systematically stronger, from 0.8 to 1.7 eV, based on the substrates (TiO_2 and ZrO_2).[14,50,55]

Finally, we emphasize that the Lewis acidity of the oxide surface controls the coverage of surface hydroxyls and thus should not be too strong for a surface to be catalytically active. Taking the γ-Al_2O_3(110) surface as the example, H_2O adsorbs dissociatively on the exposed Al_{4c} sites. The surface ends up with the termination by hydroxyl groups at the room temperature, which finally deactivates the surface. The strong acidity of Al_{4c} on γ-Al_2O_3(110) is clearly not ideal for catalysis. For the same reason, it is conceivable that a too high concentration of moisture in the Au/oxide catalyst may poison CO oxidation, since H_2O and O_2 will compete for adsorption at the interfacial cationic sites.[56]

5. Conclusion

This work represents our theoretical attempt to rationalize the CO oxidation activity on Au/γ-Al_2O_3, focusing on how moisture promotes the reaction microscopically. The majority (110) and the minority (100) surfaces of γ-Al_2O_3 are utilized as the substrates for supporting gold. We demonstrate that CO oxidation on Au/γ-Al_2O_3 occurs at the minority sites—namely, Au on γ-Al_2O_3(100)—and is governed by the H_2O-assisted reaction pathway. The main results are outlined as follows:

(i) The Au/γ-Al_2O_3(110) system shows no catalytic activity at low temperatures. All the exposed Al sites on γ-Al_2O_3(110) are blocked by dissociated H_2O due to the high activity of unsaturated Al_{4c}. Oxygen adsorbs only physically on gold. CO can adsorb on gold but cannot react with the interfacial hydroxyl.

(ii) On Au/γ-Al_2O_3(100), oxygen can adsorb at the interface with a tilted one-end Au−O−O−Al_{5c} configuration. The E_{ad} of O_2 is 0.7 eV with the coadsorption of CO and H_2O. H_2O can also adsorb molecularly at the Au/γ-Al_2O_3(100) interface with an E_{ad} of 1.00 eV, and the dissociation of H_2O is a reversible thermoneutral reaction.

(iii) In the absence of H_2O, CO oxidation follows the CO + O_2 → *cis*-OCOO → *trans*-OCOO → CO_2 + O and CO + O → CO_2 pathway. Because the atomic O is very unstable on a bare Al site, a cis-to-trans conversion of OCOO is needed to produce CO_2, and the overall barrier is 0.53 eV.

(iv) In the presence of H_2O, CO oxidation follows the CO + O_2 + H_2O → *cis*-OCOO + H_2O → CO_2 + 2OH and CO + 2OH → CO_2 + H_2O pathway. There is no atomic O involved in the H_2O-assisted pathway, and the overall barrier is only 0.25 eV. H_2O can activate the O−O bond in both the molecular oxygen and the OCOO intermediate via the H-bonding.

(v) The bonding picture for O_2 at the Au/γ-Al_2O_3 is different from that for O_2 at Au/TiO_2 and Au/ZrO_2. In the Al_2O_3 system, O_2 interacts with cationic Al via purely electrostatic interaction without the orbital mixing. Despite the lack of d-states in Al_2O_3, a modest Lewis acidity of Al cationic sites on (100) surface contributes to the O_2 adsorption and activation.

Acknowledgment. This work is supported by the NSF of China (20825311, 20773026, 20721063, J0730419), Science & Technology Community of Shanghai Municipality (08DZ2270500), and the Program for Professor of Special Appointment (Eastern Scholar) at Shanghai Institute of Higher Learning.

References and Notes

(1) Haruta, M.; Yamada, N.; Kobayashi, T.; Iijima, S. *J. Catal.* **1989**, *115*, 301.
(2) Bond, G. C.; Thompson, D. T. *Gold Bull.* **2000**, *33*, 41.
(3) Valden, M.; Lai, X.; Goodman, D. W. *Science* **1998**, *281*, 1647.
(4) Chen, M. S.; Goodman, D. W. *Science* **2004**, *306*, 252.
(5) Chen, M.; Cai, Y.; Yan, Z.; Goodman, D. W. *J. Am. Chem. Soc.* **2006**, *128*, 6341.
(6) Chen, M. S.; Goodman, D. W. *Acc. Chem. Res.* **2006**, *39*, 739.
(7) Remediakis, I. N.; Lopez, N.; Norskov, J. K. *Angew. Chem., Int. Ed.* **2005**, *44*, 1824.
(8) Lopez, N.; Norskov, J. K. *J. Am. Chem. Soc.* **2002**, *124*, 11262.
(9) Haruta, M. *Gold Bull.* **2004**, *37*, 27.
(10) Janssens, T. V. W.; Carlsson, A.; Puig-Molina, A.; Clausen, B. S. *J. Catal.* **2006**, *240*, 108.
(11) Carrettin, S.; Concepcion, P.; Corma, A.; Nieto, J. M. L.; Puntes, V. F. *Angew. Chem., Int. Ed.* **2004**, *43*, 2538.
(12) Hutchings, G. J.; Hall, M. S.; Carley, A. F.; Landon, P.; Solsona, B. E.; Kiely, C. J.; Herzing, A.; Makkee, M.; Moulijn, J. A.; Overweg, A.; Fierro-Gonzalez, J. C.; Guzman, J.; Gates, B. C. *J. Catal.* **2006**, *242*, 71.
(13) Liu, Z. P.; Hu, P.; Alavi, A. *J. Am. Chem. Soc.* **2002**, *124*, 14770.

(14) Liu, Z. P.; Gong, X. Q.; Kohanoff, J.; Sanchez, C.; Hu, P. *Phys. Rev. Lett.* **2003**, *91*, 266102.
(15) Molina, L. M.; Hammer, B. *Phys. Rev. Lett.* **2003**, *90*, 206102.
(16) Fu, Q.; Saltsburg, H.; Flytzani-Stephanopoulos, M. *Science* **2003**, *301*, 935.
(17) Date, M.; Okumura, M.; Tsubota, S.; Haruta, M. *Angew. Chem., Int. Ed.* **2004**, *43*, 2129.
(18) Daniells, S. T.; Makkee, M.; Moulijn, J. A. *Catal. Lett.* **2005**, *100*, 39.
(19) Cunningham, D. A. H.; Vogel, W.; Haruta, M. *Catal. Lett.* **1999**, *63*, 43.
(20) Costello, C. K.; Yang, J. H.; Law, H. Y.; Wang, Y.; Lin, J. N.; Marks, L. D.; Kung, M. C.; Kung, H. H. *Appl. Catal., A* **2003**, *243*, 15.
(21) Bongiorno, A.; Landman, U. *Phys. Rev. Lett.* **2005**, *95*, 106102.
(22) Yoon, B.; Hakkinen, H.; Landman, U.; Worz, A. S.; Antonietti, J. M.; Abbet, S.; Judai, K.; Heiz, U. *Science* **2005**, *307*, 403.
(23) Socaciu, L. D.; Hagen, J.; Bernhardt, T. M.; Woste, L.; Heiz, U.; Hakkinen, H.; Landman, U. *J. Am. Chem. Soc.* **2003**, *125*, 10437.
(24) Kung, H. H.; Kung, M. C.; Costello, C. K. *J. Catal.* **2003**, *216*, 425.
(25) Calla, J. T.; Davis, R. J. *Ind. Eng. Chem. Res.* **2005**, *44*, 5403.
(26) Liu, Z. P.; Wang, C. M.; Fan, K. N. *Angew. Chem., Int. Ed.* **2006**, *45*, 6865.
(27) Soler, J. M.; Artacho, E.; Gale, J. D.; Garcia, A.; Junquera, J.; Ordejon, P.; Sanchez-Portal, D. *J. Phys.: Condens. Matter* **2002**, *14*, 2745.
(28) Troullier, N.; Martins, J. L. *Phys. Rev. B: Condens. Matter* **1991**, *43*, 1993.
(29) Junquera, J.; Paz, O.; Sanchez-Portal, D.; Artacho, E. *Phys. Rev. B: Condens. Matter* **2001**, *64*, 235111.
(30) Perdew, J. P.; Burke, K.; Ernzerhof, M. *Phys. Rev. Lett.* **1996**, *77*, 3865.
(31) Anglada, E.; Soler, J. M.; Junquera, J.; Artacho, E. *Phys. Rev. B: Condens. Matter* **2002**, *66*, 205101.
(32) Wang, H. F.; Liu, Z. P. *J. Am. Chem. Soc.* **2008**, *130*, 10996.
(33) Shang, C.; Liu, Z. P. *J. Chem. Theory Comput.* **2010**, *6*, 1136.
(34) Lippens, B. C.; Deboer, J. H. *Acta Crystallogr.* **1964**, *17*, 1312.
(35) Latella, B. A.; Oconnor, B. H. *J. Am. Ceram. Soc.* **1997**, *80*, 2941.
(36) Chou, T. C.; Adamson, D.; Mardinly, J.; Nieh, T. G. *Thin Solid Films* **1991**, *205*, 131.
(37) Paglia, G.; Buckley, C. E.; Rohl, A. L.; Hart, R. D.; Winter, K.; Studer, A. J.; Hunter, B. A.; Hanna, J. V. *Chem. Mater.* **2004**, *16*, 220.
(38) Pecharroman, C.; Sobrados, I.; Iglesias, J. E.; Gonzalez-Carreno, T.; Sanz, J. *J. Phys. Chem. B* **1999**, *103*, 6160.
(39) John, C. S.; Alma, N. C. M.; Hays, G. R. *Appl. Catal.* **1983**, *6*, 341.
(40) Sohlberg, K.; Pennycook, S. J.; Pantelides, S. T. *J. Am. Chem. Soc.* **1999**, *121*, 7493.
(41) Knozinger, H.; Ratnasamy, P. *Catal. Rev.-Sci. Eng.* **1978**, *17*, 31.
(42) Alvarez, L. J.; Sanz, J. F.; Capitan, M. J.; Centeno, M. A.; Odriozola, J. A. *J. Chem. Soc., Faraday Trans.* **1993**, *89*, 3623.
(43) Digne, M.; Sautet, P.; Raybaud, P.; Euzen, P.; Toulhoat, H. *J. Catal.* **2002**, *211*, 1.
(44) Sohlberg, K.; Pantelides, S. T.; Pennycook, S. J. *J. Am. Chem. Soc.* **2001**, *123*, 26.
(45) Costello, C. K.; Guzman, J.; Yang, J. H.; Wang, Y. M.; Kung, M. C.; Gates, B. C.; Kung, H. H. *J. Phys. Chem. B* **2004**, *108*, 12529.
(46) Beaufils, J. P.; Barbaux, Y. *J. Chim. Phys. Phys.-Chim. Biol.* **1981**, *78*, 347.
(47) Nortier, P.; Fourre, P.; Saad, A. B. M.; Saur, O.; Lavalley, J. C. *Appl. Catal.* **1990**, *61*, 141.
(48) Wang, C. M.; Fan, K. N.; Liu, Z. P. *J. Catal.* **2009**, *266*, 343.
(49) Wang, C. M.; Fan, K. N.; Liu, Z. P. *J. Phys. Chem. C* **2007**, *111*, 13539.
(50) Wang, C. M.; Fan, K. N.; Liu, Z. P. *J. Am. Chem. Soc.* **2007**, *129*, 2642.
(51) Henkelman, G.; Arnaldsson, A.; Jonsson, H. *Comput. Mater. Sci.* **2006**, *36*, 354.
(52) Bader, R. F. W. *Acc. Chem. Res.* **1985**, *18*, 9.
(53) *CRC Handbook of Chemistry and Physics*; 84th ed.; LIDE., D. R., Ed.; CRC Press: Boca Raton, 2003−2004.
(54) Kung, M. C.; Davis, R. J.; Kung, H. H. *J. Phys. Chem. C* **2007**, *111*, 11767.
(55) Molina, L. M.; Rasmussen, M. D.; Hammer, B. *J. Chem. Phys.* **2004**, *120*, 7673.
(56) Date, M.; Haruta, M. *J. Catal.* **2001**, *201*, 221.

JP102477G